Engineering Science and Technology, an International Journal 19 (2016) 377–394

Contents lists available at ScienceDirect

Engineering Science and Technology, an International Journal

journal homepage: http://www.elsevier.com/locate/jestch

Full Length Article

Computational solutions for non-isothermal, nonlinear magneto-convection in porous media with hall/ionslip currents and ohmic dissipation

O. Anwar Bég [a], S. Abdul Gaffar [b,*], V. Ramachandra Prasad [c], M.J. Uddin [d]

[a] Gort Engovation Research (Medical and Aerospace Engineering Sciences), Gabriel's Wing House, 15 Southmere Avenue Great Horton, Bradford BD73NU, UK
[b] Department of Mathematics, Salalah College of Technology, Salalah, Oman
[c] Department of Mathematics, Madanapalle Institute of Technology and Science, Madanapalle 517325, India
[d] Department of Mathematics, University Sains Malaysia, Malaysia

ARTICLE INFO

Article history:
Received 1 June 2015
Received in revised form
29 July 2015
Accepted 19 August 2015
Available online 11 September 2015

Keywords:
Non-isothermal
Viscous dissipation
Non-Darcy model
Hall currents
Ionslip currents
MHD energy systems

ABSTRACT

A theoretical and numerical study is presented to analyze the nonlinear, non-isothermal, magnetohydrodynamic (MHD) free convection boundary layer flow and heat transfer in a non-Darcian, isotropic, homogenous porous medium, in the presence of Hall currents, Ionslip currents, viscous heating and Joule heating. A power-law variation is used for the temperature at the wall. The governing nonlinear coupled partial differential equations for momentum conservation in the x and z directions and heat conservation, in the flow regime are transformed from an (x, y, z) coordinate system to a (ξ,η) coordinate system in terms of dimensionless x-direction velocity (∂F/∂η) and z-direction velocity (G) and dimensionless temperature function (H) under appropriate boundary conditions. Both Darcian and Forchheimer porous impedances are incorporated in both momentum equations. Computations are also provided for the variation of the x and z direction shear stress components and also local Nusselt number. Excellent correlation is achieved with a Nakamura tridiagonal finite difference scheme (**NTM**). The model finds applications in magnetic materials processing, MHD power generators and purification of crude oils.

1. Introduction

Heat transfer in the presence of strong magnetic fields is important in various branches of magnetohydrodynamic power generation [1], nanotechnological processing [2], nuclear energy systems exploiting liquid metals [3] and blood flow control [4]. Hall currents and Ionslip effects become significant in strong magnetic fields and can considerably affect the current density in hydromagnetic heat transfer. Joule heating effects are also important and are caused by heating of the electrically-conducting fluid by the electrical current. As such considerable attention has been devoted to studying hydromagnetic convection flows with such effects. Mazumder [5] presented exact solutions for Hall current effects in rotational hydromagnetic flow due to the non-torsional oscillation of a porous plate. He investigated in detail both the steady and transient velocity fields and multiple boundary layers. Rao and Mittal [6] studied the incompressible hydromagnetic boundary layer in an MHD generator configuration using a Runge Kutta method. Hossain [7] reported on the effects of Hall currents on transient natural convection MHD boundary layer with suction at the wall using the Keller-Box numerical method. Raju and Rao [8] studied the cases of conducting and non-conducting walls for ionized hydromagnetic rotating heat transfer in a parallel plate channel with Hall currents. They showed that the temperature field is independent of partial pressure of electron gas for the case of non-conducting walls. Increasing values of rotation parameters were found to reduce the temperatures in the channel for constant Hartmann number and Hall current parameter. Sawaya et al. [9] determined experimentally the Hall parameter for electrolytic solutions in a closed loop thermosymphonic magnetohydrodynamic flow system. A one dimensional theoretical model with the measured open circuit voltage was used to quantify Hall parameter. Bhargava and Takhar [10] studied computationally the influence of Hall currents on hydromagnetic heat transfer of a viscoelastic fluid in a channel. These studies did not consider however the presence of ion-slip currents. In weaker magnetic fields, the diffusion velocity of electrons and ions is different and usually ionslip effects are neglected. However in MHD generators and industrial materials processing where the electromagnetic body forces are large (i.e. strong magnetic fields present), the diffusion velocity of the ions cannot be

* Corresponding author. Tel.: +919492078108, fax: 08571 280433.
E-mail address: abdulsgaffar0905@gmail.com (S. Abdul Gaffar).
Peer review under responsibility of Karabuk University.

http://dx.doi.org/10.1016/j.jestch.2015.08.009
2215-0986/

neglected. When both electron and ion velocities are incorporated in the analysis, the ionslip phenomenon is present and Ohm's law has to be modified accordingly. An excellent discussion of ionslip effects has been presented by Cramer and Pai [11]. Soundalgekar et al. [12] were among the first researchers to consider ionslip effects in hydromagnetic Couette heat transfer in addition to Hall currents effects. They showed that for small magnetic field parameters or high ionslip and Hall current parameters, the flow can become unstable. A reverse in flow was observed with strong Hall and ionslip effects. Strong ionslip was shown to increase temperatures whereas a rise in Hall parameter was shown to reduce temperatures. Nusselt number was shown to increase considerably with a rise in magnetic parameter but only initially to increase then decrease with ionslip parameter. Ram and Takhar [13] reported on the rotating natural convection MHD flow with Hall/ionslip current effects. Ram et al. [14] extended this study to consider the effects of oscillating wall temperature using a numerical method. Further studies of combined Hall and ionslip currents in magnetohydrodynamic heat transfer flows were provided by Takhar and Jha [15] and more recently by Elshehawey et al. [16]. M. Turkyilmazoglu [17] examined the exact solutions for the incompressible viscous MHD fluid of porous rotating disk flow with Hall current. M. Turkyilmazoglu [18] studied the exact solutions for the incompressible viscous MHD fluid of rotating disk flow with Hall current. Several studies of Joule electrical heating in MHD heat transfer flows have also appeared. Michiyoshi and Matsumoto [19] presented one of the first studies of hydromagnetic heat transfer with Joule heating. They studied the Joule heating effects on laminar parallel plate channel hydromagnetic heat transfer in the thermal entrance region. Both prescribed uniform wall heat flux and uniform wall temperature cases were considered. Wu and Cheng [20] used an eigenfunction expansion method to investigate the combined effects of Joule heating and axial conduction on thermal entry Hartmann heat transfer and flow in a parallel plate channel with different wall temperatures. They studied the case of an open circuit and considered Hartmann number up to 10 and Brinkmann numbers of 0 and −1. Mansour and Gorla [21] more recently studied the effects of Joule heating effects on transient free hydromagnetic convection in a micropolar fluid. Bég [22] studied the effects of Joule heating in MHD channel flow using a Navier–Stokes computational solver. Aissa and Mohammadein [23] more recently analyzed the effects of Joule heating and variable electric conductivity on micropolar stretching flow and heat transfer using a shooting numerical scheme. The combined effects of Hall current, magnetic induction and oblique magnetic field on MHD flow in a spinning channel with heat transfer were studied by Ghosh et al. [24]. Other studies incorporating Joule heating have been communicated by Duwairi [25] and Zueco et al. [26] who employed an electrothermal network simulation code. M. Rahimi-Gorji et al. [27] analyzed the unsteady motion of vertically falling spherical particles in non-Newtonian fluid by collocation method. Simulation of magnetic drug targeting through tracheobronchial airway in presence of an external nonuniform magnetic field using Lagrangian magnetic particle tracking was studied by O. Pourmehran et al. [28]. O. Pourmehran et al. [29] investigated the squeezing unsteady nanofluid flow between parallel plates by LSM and CM. O. Pourmehran et al. [30] studied the optimization of microchannel heat sink geometry cooled by different nanofluids using RSM analysis.

In many industrial and geophysical flows viscous dissipation effects may also arise owing to internal friction in viscous fluids which can affect temperature fields. Many studies have been reported concerning viscous heating effects in both natural and forced convection heat transfer flows. These include the articles by Gebhart and Mollendorf [31] and Soundalgekar and Pop [32] which dwell on boundary layer heat transfer. In hydromagnetic heat transfer several studies have been reported concerning viscous heating effects. Javeri [33] studied hydromagnetic heat transfer in a channel with the collective effects of Hall current, ion slip, viscous dissipation and Joule heating. Takhar and Soundalgekar [34] presented numerical solutions for the effects of Eckert number (viscous heating parameter) on hydromagnetic natural convection boundary layer flow. Other non-magnetic studies of viscous heating effects include those by Turcotte et al. [35], Basu and Roy [36], Barletta [37] and Barletta and Rossi di Schio [38]. These studies have all been restricted to purely fluid regimes. In numerous systems the medium may be a porous material. The porosity of materials is an intrinsic aspect of many chemical engineering and materials processing systems. Ceramics, batch reactors, purification systems and filtration systems all utilize porosity. Traditionally the Darcian model has been employed to analyze most convection flows in porous media. Such a model however is generally only accurate at very low Reynolds numbers and cannot simulate the inertial effects experienced at higher Reynolds numbers. Engineers have therefore extended the Darcian model to incorporate second order drag force effects generally with the Forchheimer-extended Darcian model, which is easily implemented in boundary layer heat transfer analysis. Excellent studies of Darcy–Forchheimer convection in porous media have been presented by for example, Chen and Ho [39] and also Manole and Lage [40]. O. Pourmehran et al. [41] examined the optimization of microchannel heat sink performance cooled by KKL based in saturated porous medium.

The above studies however did not consider the *collective effects* of Joule heating, Hall or ionslip currents in porous media transport phenomena. The vast majority of simulations employ a *Darcian* model [42], valid for viscous-dominated flows. In this paper therefore we shall consider the *composite effects of Joule heating, Hall and ionslip currents, and also viscous frictional heating on two-dimensional natural MHD convection in a Darcy–Forchheimer porous medium from a vertical plate with power-law variation in the wall-temperature*. Such a study has thus far not appeared in the literature and constitutes a useful extension to the current body of work on non-linear magneto-convective transport phenomena in porous media.

2. Mathematical model

We consider the steady state hydromagnetic natural convection flow of a viscous, incompressible, partially-ionized, electrically-conducting fluid flowing adjacent to a non-isothermal vertical surface in an (x, y, z) coordinate system embedded in a non-Darcy saturated porous medium. The plate surface is in the x-z plane. The z-axis coincides with the leading edge of the plate. A strong magnetic field acts parallel to the y-axis. The physical model is illustrated in Fig. 1. The magnetic Reynolds number is small for the partially-ionized fluid so that magnetic induction effects can be ignored. However, relative motion of the particles in the fluid can occur and the electron–atom collision frequency is assumed to be high enough for Hall and ionslip currents to be significant. As such, an electric current density, $\boldsymbol{J}$, is required to represent the relative motion of charged particles. Considering only the electromagnetic forces on these particles, we can utilize the generalized Ohm law. With a magnetic field, $\boldsymbol{B}$, applied normal to the electrical field $\boldsymbol{E}$, an electromagnetic force is generated normal to both $\boldsymbol{E}$ and $\boldsymbol{B}$ in the z direction. Such a force causes charged particles to migrate perpendicularly to both $\boldsymbol{E}$ and $\boldsymbol{B}$ [11]. Consequently, a component of electrical current density exists perpendicular to both $\boldsymbol{E}$ and $\boldsymbol{B}$, and this constitutes the Hall current. For a strong magnetic field $\mathbf{B}$ the diffusion velocity of the ions will be significant, constituting the ionslip effect. From the equation of conservation of electrical charge:

$$\nabla \cdot \mathbf{J} = 0 \tag{1}$$

where $\boldsymbol{J} = (J_x, J_y, J_z)$. Since the plate is not composed of electrically-conducting material, electrical charge at the surface of the plate is

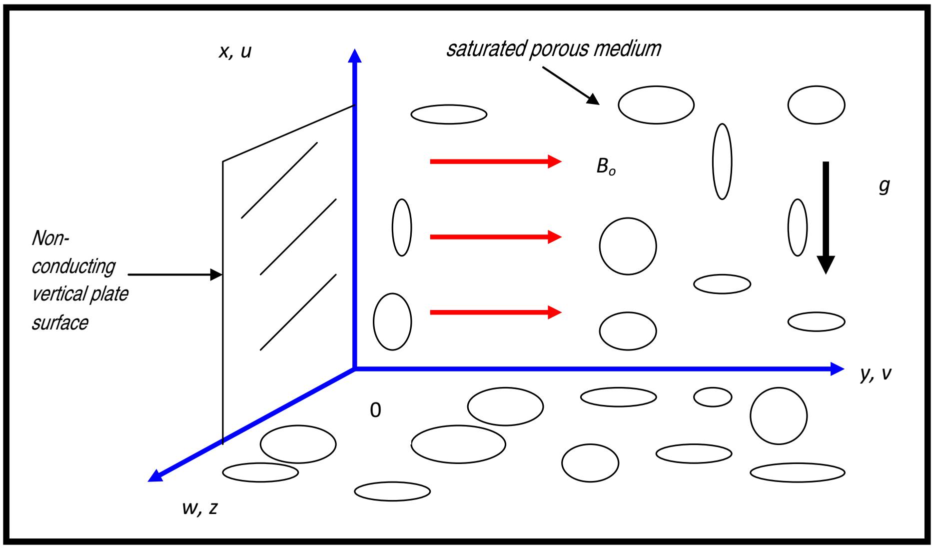

Fig. 1. Physical model and coordinate system.

constant and zero i.e. $J_y \to 0$. Consequently we can assume that $J_y = 0$ throughout the fluid-saturated porous medium. The magnetic field acts only in the y-direction with a component, B_0. The surface temperature of the heated plate is modeled using a power-law for non-isothermal behavior as follows:

$$T_w(x) = T_\infty + Ax^n \tag{2}$$

where $T_w(x)$ is variable wall temperature, T_∞ is the free-stream temperature (outside the boundary layers), A designates a constant and n is a power-law exponent. We implement a Darcy–Forchheimer model which is a second order relationship defining the pressure gradient as:

$$\nabla p = -aU + bU^2 \tag{3}$$

where U denotes velocity, ∇p is pressure gradient, a and b are constants defined by $a = \mu/K$ and b is a function of the geometry of porous medium i.e. b is the Forchheimer form-drag parameter for quadratic effects and μ is the dynamic viscosity of the partially-ionized fluid, K is permeability of the porous medium. We assume that the density of the partially-ionized fluid can be taken as constant i.e. the flow is incompressible. In addition, we implement the Boussinesq approximation which implies that all thermodynamic quantities of the fluid-saturated medium are constant, except for the buoyancy term, which is retained in the x-direction momentum conservation equations. We have assumed that the porous medium is homogenous and isotropic so that only a single permeability is needed to simulate hydraulic conductivity. Under these physical conditions, with viscous and Joule heating effects incorporated, the flow regime in an [x, y, z] coordinate system can be represented by the following boundary-layer equations:

Mass Conservation

$$\frac{\partial u}{\partial x} + \frac{\partial v}{\partial y} = 0 \tag{4}$$

x-direction Momentum Conservation

$$u\frac{\partial u}{\partial x} + v\frac{\partial u}{\partial y} = \nu\frac{\partial^2 u}{\partial y^2} + g\beta[T - T_\infty] - \nu\frac{u}{K} - b\frac{u^2}{K} - \frac{\sigma B_o^2}{\rho(\alpha_e^2 + \beta_e^2)}(\alpha_e u + \beta_e w) \tag{5}$$

z-direction Momentum Conservation

$$u\frac{\partial w}{\partial x} + v\frac{\partial w}{\partial y} = \nu\frac{\partial^2 w}{\partial y^2} - \nu\frac{w}{K} - b\frac{w^2}{K} + \frac{\sigma B_o^2}{\rho(\alpha_e^2 + \beta_e^2)}(\beta_e u - \alpha_e w) \tag{6}$$

Energy (Heat) Conservation

$$u\frac{\partial T}{\partial x} + v\frac{\partial T}{\partial y} = \frac{k}{\rho c_p}\frac{\partial^2 T}{\partial y^2} + \frac{\nu}{c_p}\left[\left(\frac{\partial u}{\partial y}\right)^2 + \left(\frac{\partial w}{\partial y}\right)^2\right] + \frac{\sigma B_o^2}{\rho c_p(\alpha_e^2 + \beta_e^2)}(u^2 + w^2) \tag{7}$$

where u, v, w are velocity components in the x, y, z directions, T is the fluid temperature, ν is kinematic viscosity of the partially-ionized fluid, g is acceleration due to gravity, β is the coefficient of volume expansion, ρ is density of the electrically-conducting fluid, k is thermal conductivity of the fluid-saturated porous medium, c_p is specific heat capacity of the fluid under isobaric conditions, σ is the fluid electrical conductivity ($=e^2 t_e n_e/m_e$), e denotes the electron charge, t_e is the electron collision time, n_e is the electron number density, m_e is the electron mass, $\alpha_e = 1 + \beta_i\beta_e$, $\beta_i = \dfrac{e n_e B_o}{\left[\left(1+\dfrac{n_e}{n_a}\right)K_{ai}\right]}$ is the ion-slip parameter, $\beta_e = \omega_e t_e$ is the Hall current parameter, ω_e is the electron frequency ($=eB_o/m_e$), n_a is the neutral particle number density and K_{ai} is the friction coefficient between the ions and neutral particles in the flow. In equation (5) the third and fourth terms on the right hand sides are the *x-direction Darcian drag force* and the *x-direction Forchheimer quadratic drag*. Similar terms are incorporated for the z-direction components of these forces in equation (6). We note that the viscous heating term in (7) comprises the square of two velocity gradients $\left[\left(\frac{\partial u}{\partial y}\right)^2 + \left(\frac{\partial v}{\partial y}\right)^2\right]$ which is a realistic approximation, supported by the seminal study of Gebhart and Mollendorf [31]. The corresponding initial conditions and boundary conditions for the flow regime are prescribed as follows, which include the conventional no-slip boundary condition at the plate surface:

$$\text{At } y = 0: \quad u = 0, w = 0, T = T_w(x) = T_\infty + Ax^n \tag{8a}$$

$$\text{As } y \to \infty: \quad u \to 0, w \to 0, T \to T_\infty \tag{8b}$$

3. Transformation of model

In order to facilitate a numerical solution to the boundary value problem i.e. coupled non-linear partial differential equations (5) to (7) under conditions (8a, b), we introduce the following transformations and non-dimensional variables:

$$\eta=\frac{Cy}{x^{1/4}},\quad \xi=\frac{x^{1/2}}{L^{1/2}},\quad \Psi=4\nu Cx^{3/4}F,\quad u=\frac{\partial\Psi}{\partial y},\quad v=-\frac{\partial\Psi}{\partial x},\quad Da=\frac{K}{L^2},$$
$$w=4\nu C^2x^{1/2}G,\quad C=\left\{\frac{g\beta[T_w(x)-T_\infty]}{4\nu^2}\right\}^{1/4},\quad H=\frac{T-T_\infty}{T_w(x)-T_\infty},$$
$$\Pr=\frac{\mu c_p}{k},\quad Fs=\frac{b}{L},\quad Gr_x=\frac{g\beta x^3[T_w(x)-T_\infty]}{\nu^2},\quad Ec=\frac{4L\nu^2C^4}{c_p[T_w(x)-T_\infty]},$$
$$Nm=\frac{\sigma B_o^2L^{1/2}}{2\rho\nu C^2},\tag{9}$$

All the parameters have been defined in nomenclature. Our transport equations now reduce to the following trio of non-linear, coupled, partial differential equations for F, G, H in terms of the independent variables ξ,η:

Primary Momentum Conservation

$$\frac{\partial^3F}{\partial\eta^3}+(n+3)F\left[\frac{\partial^2F}{\partial\eta^2}\right]-2(n+1)\left[\frac{\partial F}{\partial\eta}\right]^2+H-\frac{2Nm}{[\alpha_e{}^2+\beta_e{}^2]}\xi\left[\alpha_e\frac{\partial F}{\partial\eta}+\beta_eG\right]-\frac{2}{DaGr_x{}^{1/2}}\xi^4\frac{\partial F}{\partial\eta}-\frac{4Fs}{Da}\xi^2\left[\frac{\partial F}{\partial\eta}\right]^2=2\xi\left[\frac{\partial F}{\partial\eta}\frac{\partial^2F}{\partial\xi\partial\eta}-\frac{\partial^2F}{\partial\eta^2}\frac{\partial F}{\partial\xi}\right]\tag{10}$$

Secondary (Cross-Flow) Momentum Conservation

$$\frac{\partial^2G}{\partial\eta^2}-2(n+1)G\left[\frac{\partial F}{\partial\eta}\right]+(n+3)F\left[\frac{\partial G}{\partial\eta}\right]-\frac{2Nm}{[\alpha_e{}^2+\beta_e{}^2]}\xi\left[\alpha_eG-\beta_e\frac{\partial F}{\partial\eta}\right]-\frac{2}{DaGr_x{}^{1/2}}\xi^4G-\frac{4Fs}{Da}\xi^2G^2=2\xi\left[\frac{\partial F}{\partial\eta}\frac{\partial G}{\partial\xi}-\frac{\partial G}{\partial\eta}\frac{\partial F}{\partial\xi}\right]\tag{11}$$

Energy Conservation

$$\frac{1}{\Pr}\frac{\partial^2H}{\partial\eta^2}+(n+3)F\left[\frac{\partial H}{\partial\eta}\right]-4n\left[\frac{\partial F}{\partial\eta}\right]H+\xi^2Ec\left[\left(\frac{\partial^2F}{\partial\eta^2}\right)^2+\left(\frac{\partial G}{\partial\eta}\right)^2\right]+\frac{2Nm\,Ec}{[\alpha_e{}^2+\beta_e{}^2]}\xi^3\left[\left(\frac{\partial F}{\partial\eta}\right)^2+G^2\right]=2\xi\left[\frac{\partial F}{\partial\eta}\frac{\partial H}{\partial\xi}-\frac{\partial H}{\partial\eta}\frac{\partial F}{\partial\xi}\right]\tag{12}$$

The corresponding transformed boundary conditions now become:

$$\frac{\partial F(\xi,0)}{\partial\eta}=0;\quad (n+3)F(\xi,0)+2\xi\frac{\partial F(\xi,0)}{\partial\xi}=0;\quad G(\xi,0)=0;\quad H(\xi,0)=1\tag{13a}$$

$$\frac{\partial F(\xi,\infty)}{\partial\eta}=0;\quad G(\xi,\infty)=0;\quad H(\xi,\infty)=0\tag{13b}$$

The present model therefore constitutes a two-point boundary value problem for which we shall derive Keller box numerical solutions in due course.

4. Engineering parameters

For practical design purposes in MHD energy systems a number of engineering parameters provide important descriptions of the wall transport processes. The local heat flux, $q_w(x)$, local heat transfer coefficient, $h(x)$ at the wall and the local Nusselt number, Nu_x, are defined as:

$$q_w(x)=-k\left.\frac{\partial T}{\partial y}\right|_{y=0}=-k[T_w(x)-T_\infty]\frac{C}{x^{1/4}}\frac{\partial H(\xi,0)}{\partial\eta}\tag{14}$$

$$h(x)=\frac{q_w(x)}{[T_w(x)-T_\infty]}=-k\frac{C}{x^{1/4}}\frac{\partial H(\xi,0)}{\partial\eta}\tag{15}$$

$$Nu_x=\frac{xh(x)}{k}=-\frac{1}{\sqrt{2}}Gr_x{}^{1/4}\frac{\partial H(\xi,0)}{\partial\eta}\tag{16}$$

The local shear stress components in the x and z-directions respectively, namely, τ_{wx} and τ_{wz}, may be defined using the relations:

$$\tau_{wx}=4\mu\nu C^3x^{1/4}\frac{\partial^2F(\xi,0)}{\partial\eta^2}=\sqrt{2}\mu\nu\frac{Gr_x{}^{3/4}}{x^2}\frac{\partial^2F(\xi,0)}{\partial\eta^2}\tag{17}$$

$$\tau_{wz}=4\mu\nu C^3x^{1/4}\frac{\partial G(\xi,0)}{\partial\eta}=\sqrt{2}\mu\nu\frac{Gr_x{}^{3/4}}{x^2}\frac{\partial G(\xi,0)}{\partial\eta}\tag{18}$$

To provide a benchmark for numerical solutions, a number of special cases of the general flow model can be retrieved from equations (10) to (12) with conditions (13a, b). Setting $n\to 0$, the power-law temperature variation reduces to the isothermal case. With $Fs\to 0$, inertial effects disappear and only a bulk porous matrix resistance (Darcian) acts on the partially-ionized fluid in the porous medium. With $Da\to\infty$, the regime permeability becomes infinite and the porous fibers vanish in the limit. The model contracts to purely fluid hydromagnetic convection flow. For the case of $Ec\to 0$, both viscous heating and Joule electric current heating terms vanish in the energy conservation equation. Finally with absence of magnetic field effects, $Nm\to 0$, which also negates Hall current and ionslip effects in the momentum equations.

5. Keller Box computational solutions

The Keller-Box implicit difference method is utilized to solve the nonlinear boundary value problem defined by eqns. (10)–(12) with boundary conditions (13). Although other powerful numerical methods have been developed in fluid mechanics including differential transform quadrature [20] and MAPLE shooting methods [42], for *parabolic* problems (of which boundary layer flows are an excellent example), Keller's box technique [43] remains extremely popular since it easily solves two-coordinate problems (partial differential families of equations). Although Keller's box scheme was developed over four decades ago, it has witnessed a recent resurge in implementation. Recent areas in which box scheme has been employed include subsonic thruster flows [44], aircraft wing aerodynamics [45], stationary convective-diffusion flows [46], magnetohydrodynamics [47], wavy surface convection flows [48], nanofluids [49], drainage sheet flows [50] and rotating flows [51]. Further applications include magneto-convection [52], double-diffusive convection [53] and fuel cell modeling [54], tangent hyperbolic fluid [55]. The Keller-Box discretization is *fully coupled* at each step which reflects the physics of parabolic systems – which are also fully coupled. Discrete calculus associated with the Keller-Box scheme has also been shown to be fundamentally different from all other mimetic (physics capturing) numerical methods, as elaborated by Keller [43]. The Keller Box Scheme comprises four stages:

1) Decomposition of the Nth order partial differential equation system to N first order equations.
2) Finite Difference Discretization.
3) Quasilinearization of Non-Linear Keller Algebraic Equations.

Table 1
Values of C_{fx}, C_{gx} and Nu_x for different Da and ξ ($\beta_i = 0.4$, $Nm = 0.5$, $\beta e = 0.5$, $Gr = 1.0$, $n = 0.3$, $Ec = Fs = 0.1$, $Pr = 1.0$).

Da	$\xi = 1.0$			$\xi = 2.0$			$\xi = 3.0$		
	C_{fx}	C_{gx}	Nu_x	C_{fx}	C_{gx}	Nu_x	C_{fx}	C_{gx}	Nu_x
0.01	0.0893	0.0017	0.1308	0.0242	–0.0003	0.0867	0.0113	0.0009	–0.0046
0.05	0.1954	0.0142	0.1305	0.0533	0.0045	0.1407	0.0246	0.0012	0.1421
0.1	0.2693	0.0187	0.1571	0.0748	0.0106	0.1414	0.0344	0.0026	0.1464
0.15	0.3210	0.0205	0.1856	0.0910	0.0153	0.1428	0.0418	0.0043	0.1425
0.2	0.3612	0.0215	0.2128	0.1047	0.0185	0.1466	0.0481	0.0061	0.1424
0.25	0.3938	0.0220	0.2346	0.1167	0.0208	0.1489	0.0536	0.0079	0.1417
0.3	0.4211	0.0224	0.2530	0.1275	0.0225	0.1521	0.0586	0.0098	0.1407

Table 2
Values of C_{fx}, C_{gx} and Nu_x for different Fs and ξ ($\beta_i = 0.4$, $\beta e = 0.5$, $N_m = 0.5$, $Gr = 1.0$, $n = 0.3$, $Ec = Da = 0.1$, $Pr = 1.0$).

Fs	$\xi = 1.0$			$\xi = 2.0$			$\xi = 3.0$		
	C_{fx}	C_{gx}	Nu_x	C_{fx}	C_{gx}	Nu_x	C_{fx}	C_{gx}	Nu_x
0.01	0.2698	0.0190	0.1567	0.0748	0.0108	0.1402	0.0344	0.0026	0.1455
0.05	0.2702	0.0189	0.1569	0.0748	0.0107	0.1402	0.0344	0.0026	0.1455
0.1	0.2705	0.0187	0.1571	0.0748	0.0106	0.1404	0.0344	0.0026	0.1464
1.0	0.2706	0.0167	0.1595	0.0749	0.0088	0.1410	0.0345	0.0025	0.1482
5.0	0.2708	0.0118	0.1641	0.0763	0.0061	0.1503	0.0359	0.0022	0.1794
7.0	0.2710	0.0105	0.1661	0.0778	0.0055	0.1608	0.0375	0.0021	0.2169
10.0	0.2713	0.0091	0.1719	0.0832	0.0049	0.2032	0.0428	0.0019	0.3570

4) Block-tridiagonal Elimination solution of the Linearized Keller Algebraic Equations.

6. Stability and convergence of Keller Box method

In laminar boundary layer calculations, the wall shear stress parameter $v(x, 0)$ is commonly used as the convergence criterion [56]. This is probably because in boundary layer calculations, it is found that the greatest error usually appears in the wall shear stress parameter. Different criterion is used for turbulent flow problem. Throughout the study of this paper, the convergence criterion is used as it is efficient, suitable and the best. Calculations are stopped when

$$\left|\delta v_0^{(i)}\right| < \varepsilon_1$$

where ε_1 is a small prescribed value.

7. Keller Box computational results

Comprehensive solutions have been obtained and are presented in Tables 1–4 and Figs. 2–11. The numerical problem comprises two independent variables (ξ,η), three dependent fluid dynamic variables (F, G, H) and different thermo-physical and body force control parameters, namely, β_e, β_i, N_m, n, Pr, Da, Fs, Gr_x, Ec. The following default parameter values i.e. $\beta_e = 0.5$, $\beta_i = 0.4$, $N_m = 0.5$, $n = 0.3$, $Pr = Gr_x = 1.0$, $Ec = Da = Fs = 0.1$ are prescribed (unless otherwise stated). Validation with Nakamura's tridiagonal finite difference method (**NTM**) [57] is provided in the next section with Tables 3 and 4.

8. Validation with Nakamura tridiagonal method (NTM)

To validate the present solutions, we have also utilized an efficient finite difference procedure of the implicit type, originally developed by Nakamura [49] to solve the seventh order nonlinear partial differential boundary value problem defined by eqns. (10)–(12) under boundary conditions (13a,b). As with other difference schemes, a reduction of the higher order differential equations arising is intrinsic also to the Nakamura tridiagonal method (**NTM**). **NTM** is also particularly accurate at simulating parabolic problems as exemplified by boundary layer flows. Applications of **NTM** in micromorphic and other non-Newtonian flows include flat plate micropolar convection [58], Ostwald–de Waele shear-thinning plume flows [59], centrifugal heart pump hemodynamics [60], viscoelastic biopolymer wedge flows [61]. More recently NTM has been successfully utilized in studying nanofluid bioconvection of oxytactic micro-organisms in a microbial porous media fuel cell by Bég et al.

Table 3
KBM and **NTM** solutions compared for C_{fx}, C_{gx} and Nu_x with different β_e and ξ ($\beta_i = 0.4$, $Nm = 0.5$, $n = 0.3$, $Gr = 1.0$, $Ec = Da = Fs = 0.1$, $Pr = 1.0$).

β_e	$\xi = 1.0$			$\xi = 1.0$		
	C_{fx} KBM	C_{gx} KBM	Nu_x KBM	C_{fx} NTM	C_{gx} NTM	Nu_x NTM
0.2	0.2685	0.0101	0.1570	0.2686	0.0102	0.1570
0.5	0.2693	0.0187	0.1571	0.2692	0.0188	0.1570
1.0	0.2703	0.0225	0.1571	0.2703	0.0226	0.1571
1.5	0.2710	0.0214	0.1571	0.2709	0.0215	0.1571
2.0	0.2713	0.0193	0.1572	0.2712	0.0192	0.1572
2.5	0.2716	0.0173	0.1572	0.2715	0.0172	0.1572
3.0	0.2718	0.0155	0.1572	0.2717	0.0154	0.1572
5.0	0.2721	0.0107	0.1572	0.2722	0.0108	0.1572
8.0	0.2723	0.0072	0.1572	0.2724	0.0073	0.1572
10.0	0.2723	0.0059	0.1572	0.2723	0.0060	0.1572

Table 4
KBM and **NTM** solutions compared for C_{fx}, C_{gx} and Nu_x with different n and ξ ($\beta_e = 0.4$, $Nm = 0.5$, $n = 0.3$, $Gr = 1.0$, $Ec = Da = Fs = 0.1$, $Pr = 1.0$).

β_i	$\xi = 2.0$			$\xi = 2.0$		
	C_{fx} KBM	C_{gx} KBM	Nu_x KBM	C_{fx} NTM	C_{gx} NTM	Nu_x NTM
0.1	0.0745	0.0130	0.1406	0.0744	0.0131	0.1405
0.5	0.0745	0.0099	0.1404	0.0745	0.0100	0.1404
1.0	0.0746	0.0073	0.1402	0.0746	0.0072	0.1402
1.5	0.0746	0.0056	0.1401	0.0746	0.0054	0.1401
2.0	0.0747	0.0044	0.1400	0.0747	0.0043	0.0746
3.0	0.0747	0.0030	0.1398	0.0747	0.0031	0.0746
4.0	0.0748	0.0021	0.1397	0.0747	0.0022	0.0747
7.0	0.0748	0.0010	0.1395	0.0748	0.0011	0.0748
10.0	0.0749	0.0006	0.1394	0.0749	0.0059	0.0750

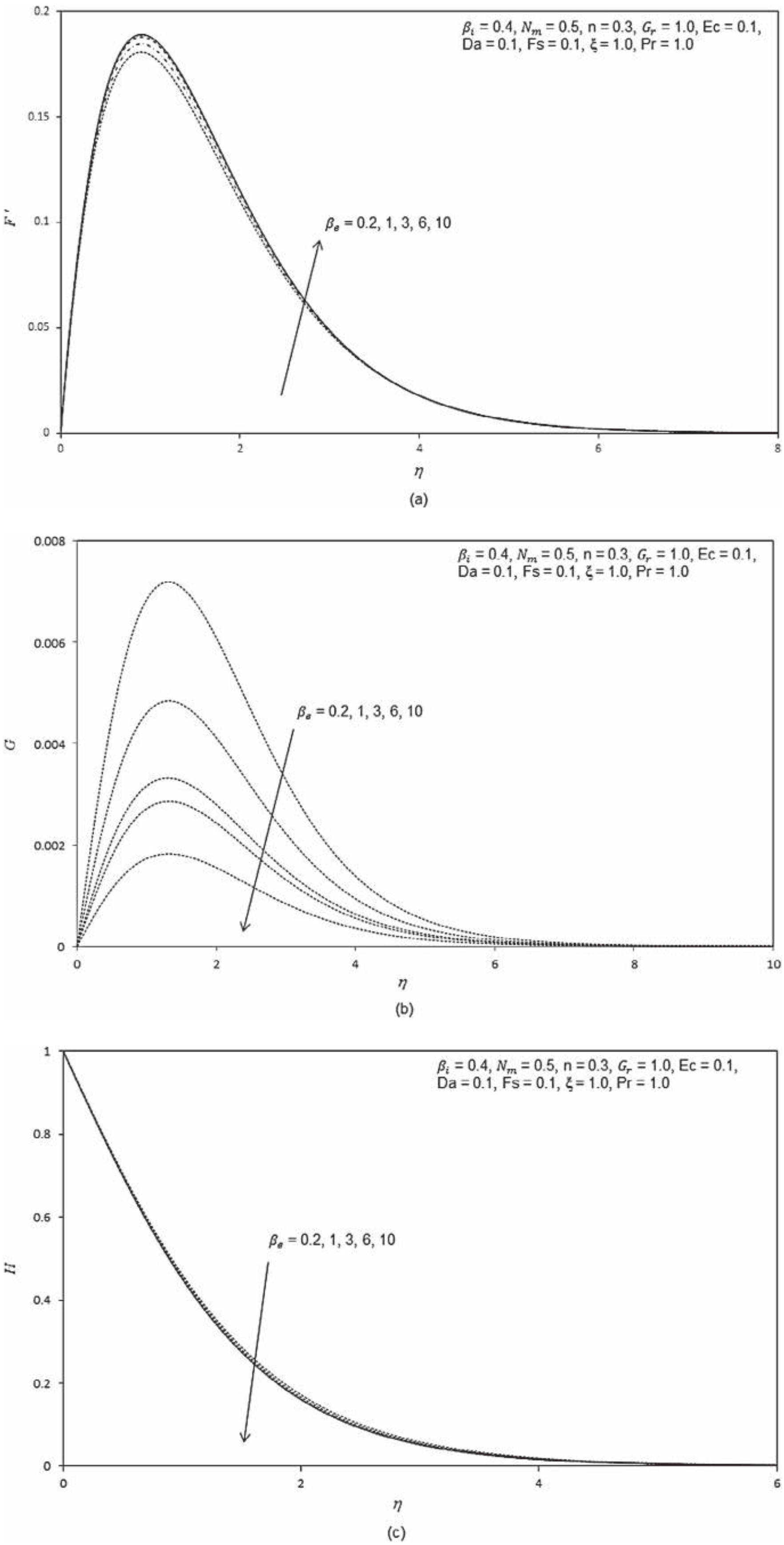

Fig. 2. (a) Influence of β_e on primary velocity profiles. (b) Influence of β_e on secondary velocity profiles. (c) Influence of β_e on temperature profiles.

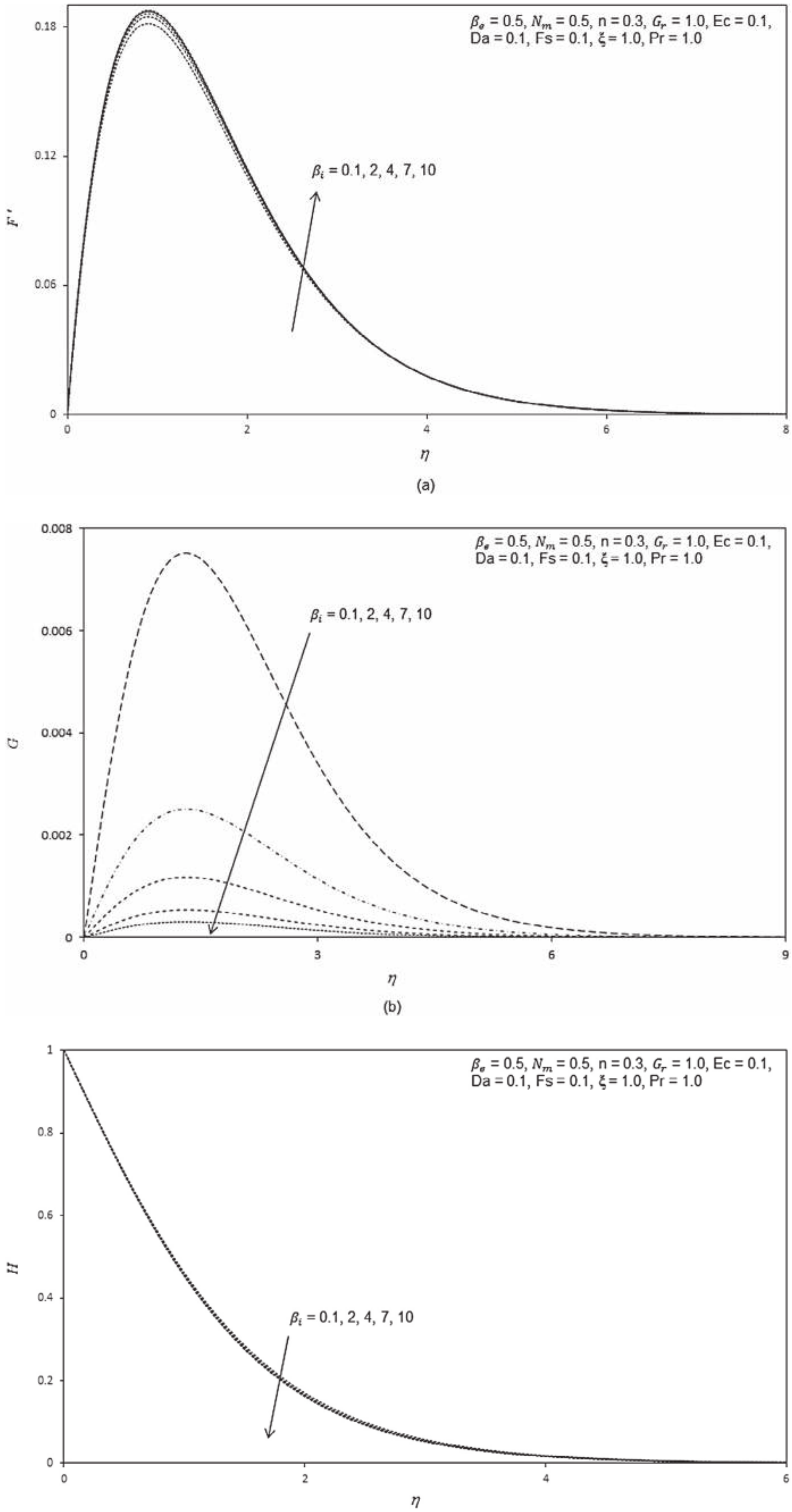

Fig. 3. (a) Influence of β_i on primary velocity profiles. (b) Influence of β_i on secondary velocity profiles. (c) Influence of β_i on temperature profiles.

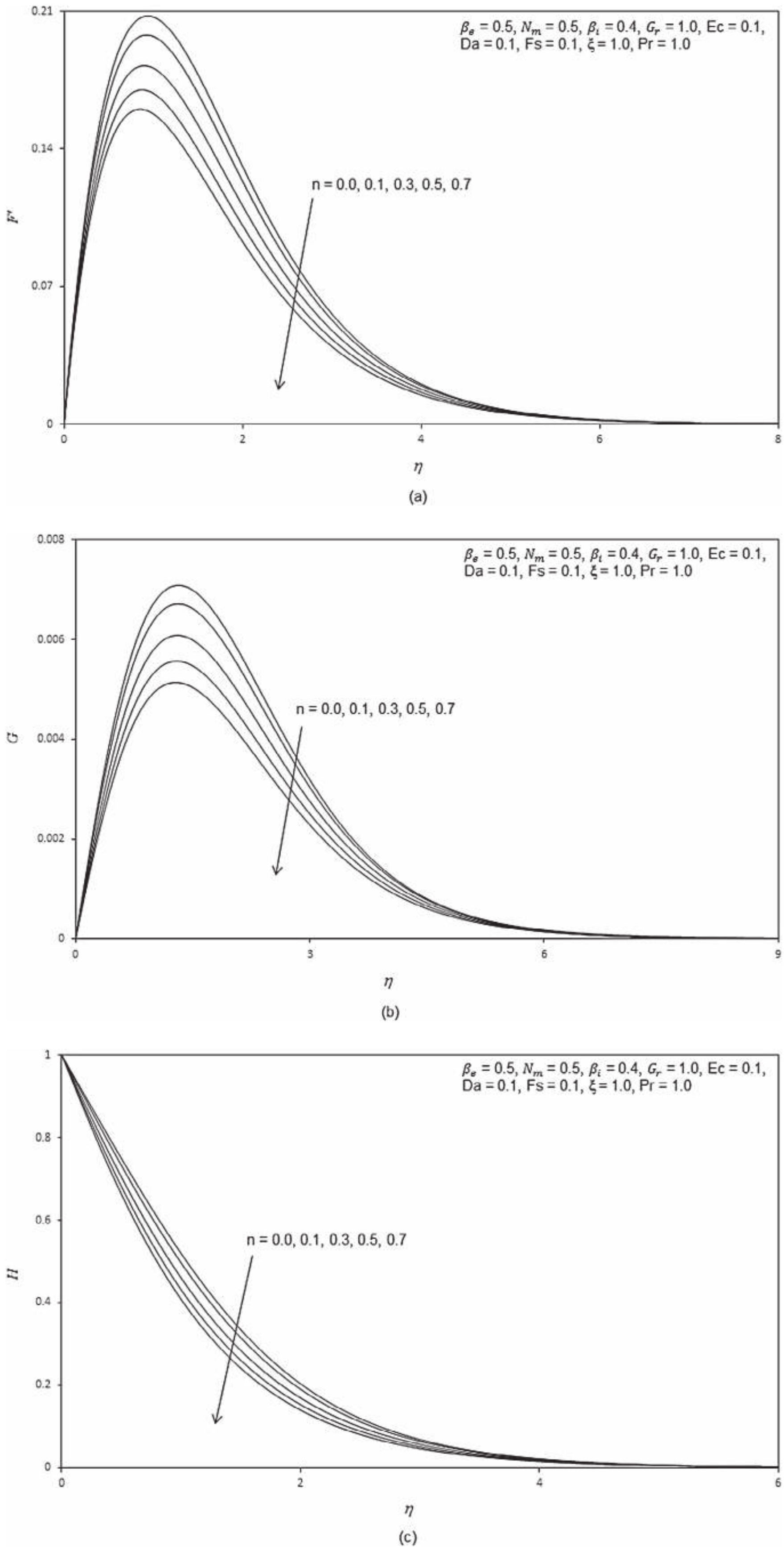

Fig. 4. (a) Influence of n on primary velocity profiles. (b) Influence of n on secondary velocity profiles. (c) Influence of n on temperature profiles.

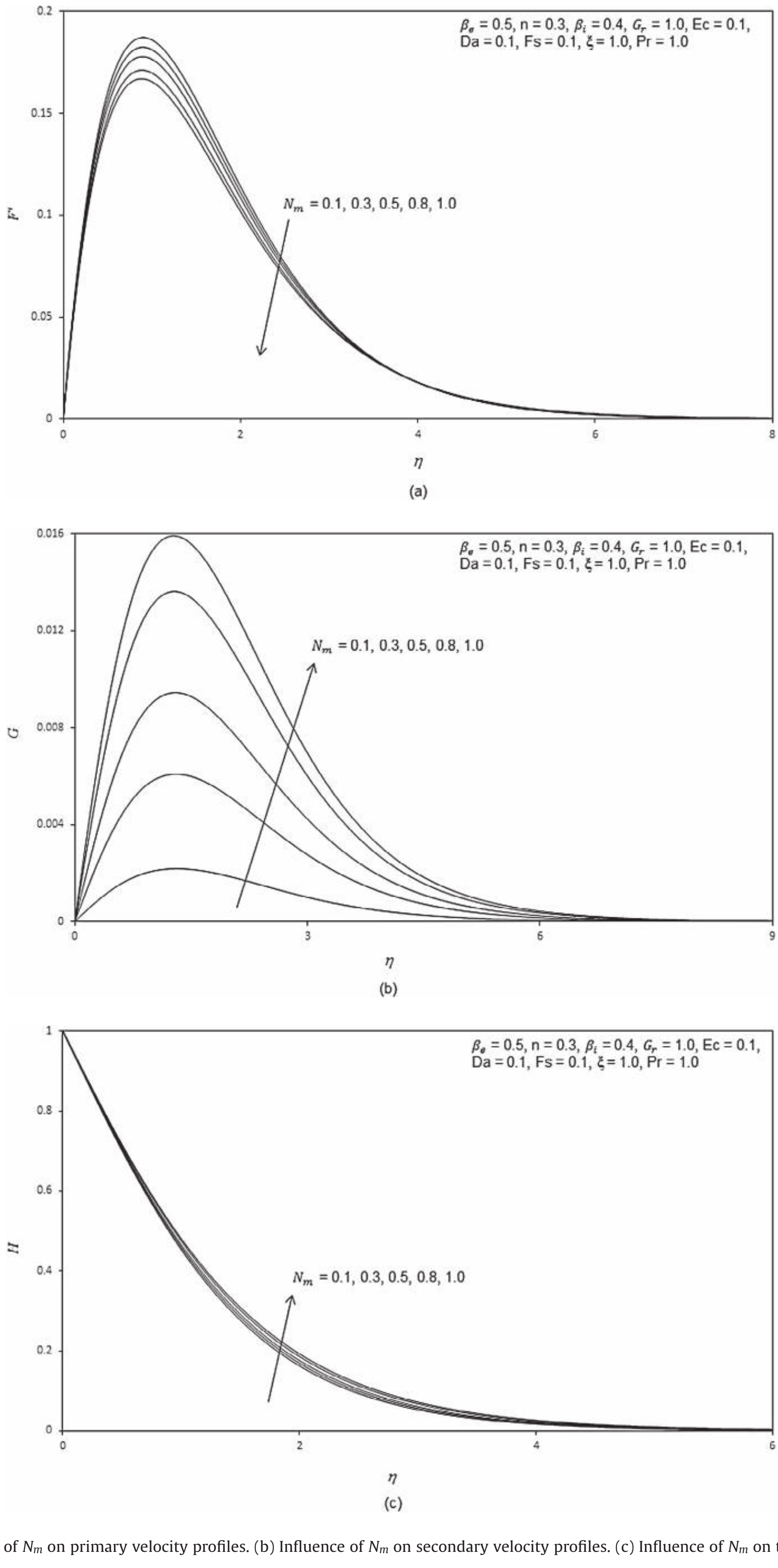

Fig. 5. (a) Influence of N_m on primary velocity profiles. (b) Influence of N_m on secondary velocity profiles. (c) Influence of N_m on temperature profiles.

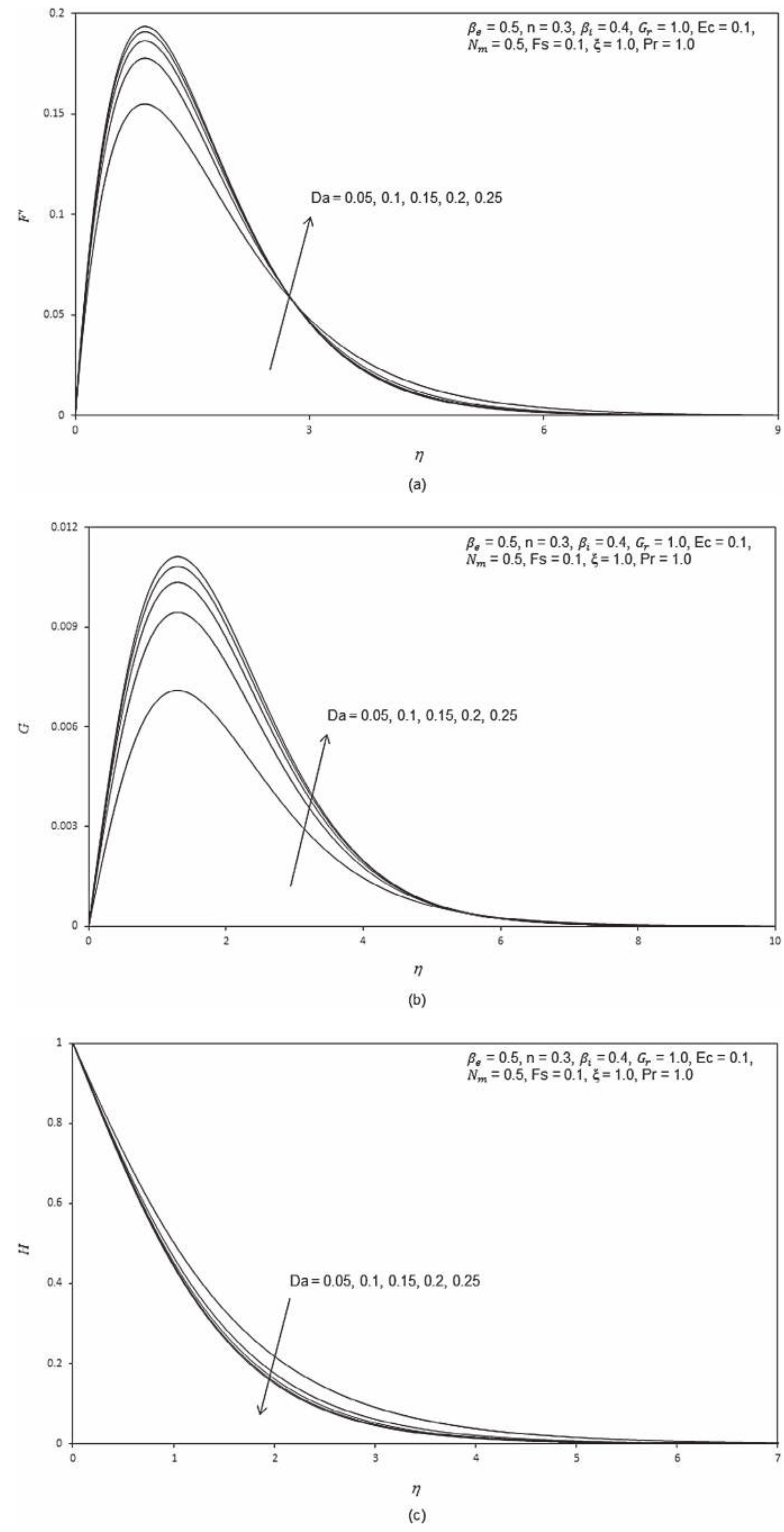

Fig. 6. (a) Influence of Da on primary velocity profiles. (b) Influence of Da on secondary velocity profiles. (c) Influence of Da on temperature profiles.

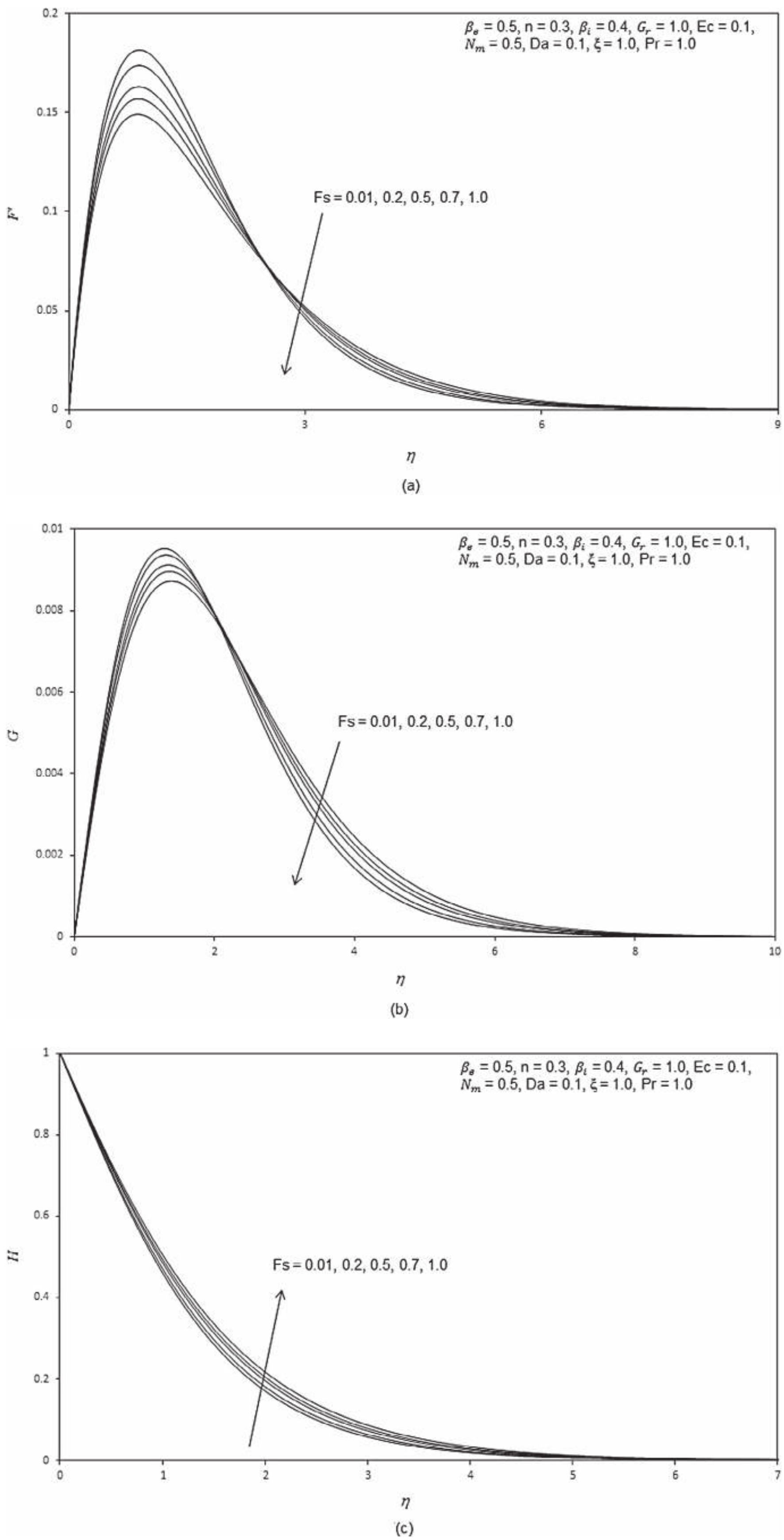

Fig. 7. (a) Influence of Fs on primary velocity profiles. (b) Influence of Fs on secondary velocity profiles. (c) Influence of Fs on temperature profiles.

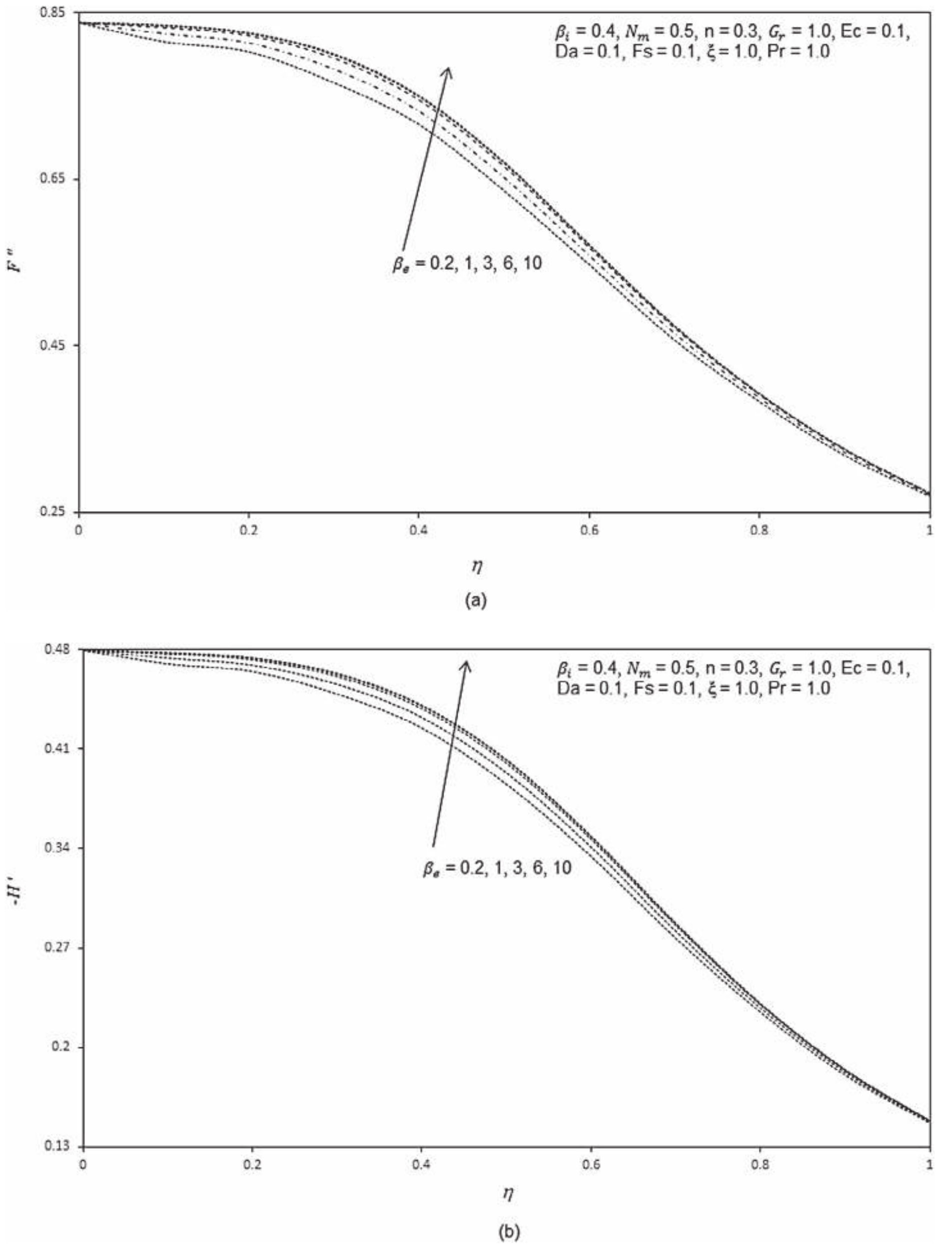

Fig. 8. (a) Influence of β_e on skin friction coefficient results. (b) Influence of β_e on Nusselt number results.

[62] and micropolar conducting biopolymer enrobing flows [63]. **NTM** works well for both one-dimensional (ordinary differential equation systems) and two-dimensional (partial differential) non-similar flows. **NTM** entails a combination of the following aspects. In the computations both an inner and outer loop is required, the former to advance the solution in the η-direction, and the latter to advance it in the ξ-direction. The flow domain is discretized using an equi-spaced finite difference mesh in the (ξ,η)-directions. The partial derivatives for F, G, H with respect to ξ,η are evaluated by central difference approximations. A double iteration loop based on the method of successive substitution is employed. The finite difference discretized equations are solved as a *linear* second order boundary value problem on the ξ,η-domain. All the conservation equations, except the primary momentum eqn. (10), are *second order* equations, and for these eqns., viz (11), (12) only a *direct* substitution is needed. Setting:

$$P = F^{//} \tag{19}$$

$$Q = G \tag{20}$$

$$R = H \tag{21}$$

The eqns. (10)–(12) then assume the form:
Nakamura primary momentum equation:

$$A_1P^{//} + B_1P^{/} + C_1P = S_1 \tag{22}$$

Nakamura secondary momentum equation:

$$A_2Q^{//} + B_2Q^{/} + C_2Q = S_2 \tag{23}$$

Nakamura energy equation:

$$A_3S^{//} + B_3S^{/} + C_3S = S_3 \tag{24}$$

where $A_{i=1...3}$, $B_{i=1...3}$, $C_{i=1...3}$ are the *Nakamura matrix coefficients*, $S_{i=1...3}$ are the *Nakamura source terms* containing a mixture of variables and

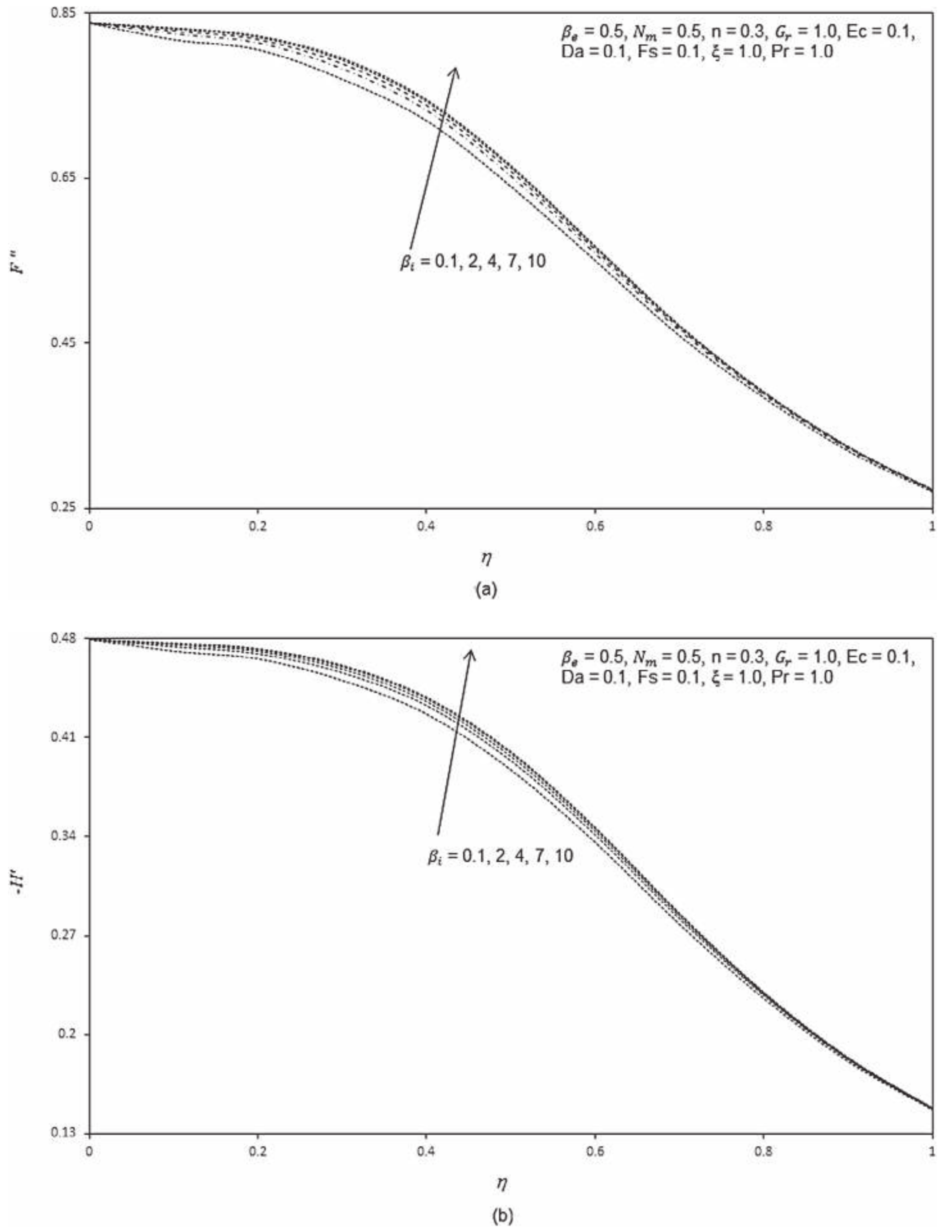

Fig. 9. (a) Influence of β_i on skin friction coefficient results. (b) Influence of β_i on Nusselt number results.

derivatives associated with the variables (omitted for brevity). The Nakamura eqns. (22)–(24) are transformed to finite difference equations and these are orchestrated to form a tridiagonal system which is solved iteratively. Tables 3 and 4 document the comparison of **KBM** and **NTM** solutions for the effects of Hall current parameter (β_e) and ionslip parameter (β_i) in addition to ξ-coordinate on *primary shear stress function, secondary shear stress function and heat transfer rate.* Excellent agreement is achieved. Confidence in the Keller-box solutions is therefore high.

9. Discussion

In all the computations a highly permeable medium is studied and Darcy numbers are very high for this reason. Although Eckert number (viscous heating) is included we do not study it explicitly as this has been reported in many other studies. The computations however do simulate dissipative flows with Joule heating (Ohmic dissipation) as *Ec* is prescribed as 0.1 throughout. Prandtl number is set as unity to correspond to ionized gases [64]. In the graphs $F = f$, $G = g$, $H = \theta$.

Fig. 2a–c depicts the evolution of primary velocity (F'), secondary velocity (G) and temperature (H) functions with a variation in Hall current parameter, β_e. This parameter generates the cross flow effect in magnetohydrodynamics [64]. The Hall current parameter arises in both the primary and secondary momentum eqns. (10), (11) via the *cross-flow* coupling terms, $-\frac{2Nm}{[\alpha_e^2+\beta_e^2]}\xi\left[\alpha_e\frac{\partial F}{\partial\eta}+\beta_e G\right]$ and $-\frac{2Nm}{[\alpha_e^2+\beta_e^2]}\xi\left[\alpha_e G-\beta_e\frac{\partial F}{\partial\eta}\right]$. It arises in quadratic form as a denominator i.e. $-\frac{2Nm}{[\alpha_e^2+\beta_e^2]}$ in both and is coupled to the secondary velocity, G, in the former, and to the primary velocity, $\frac{\partial F}{\partial\eta}$ in the latter. The effect is for acceleration in the primary flow with greater Hall current parameter, as observed in Fig. 2a. The peak velocity is attained some

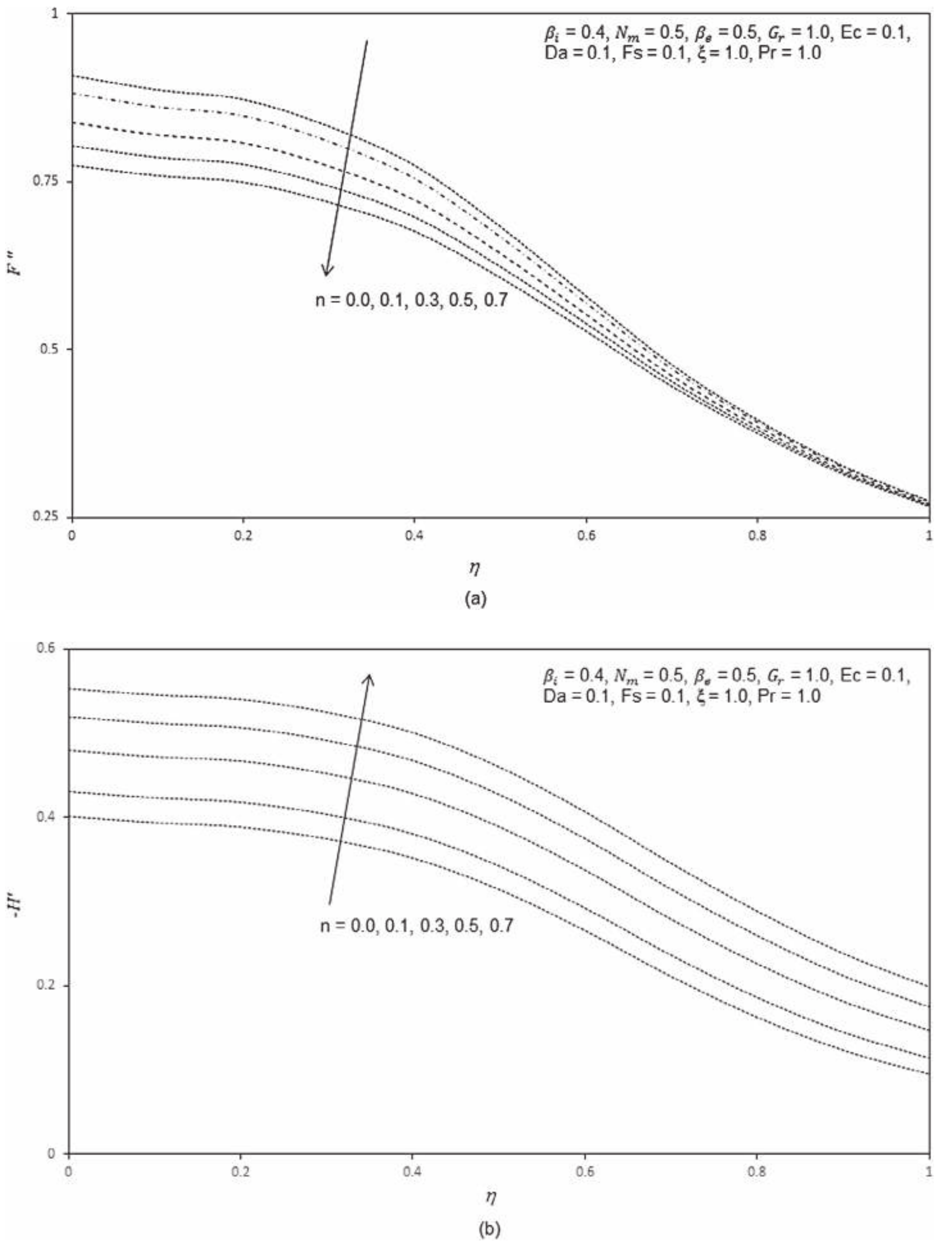

Fig. 10. (a) Influence of n on skin friction coefficient results. (b) Influence of n on Nusselt number results.

distance from the plate surface. The primary velocity profiles in all cases converge asymptotically to vanishing free stream velocity, demonstrating that a sufficiently large infinity is prescribed in the computations. Momentum supplied to accelerate the primary flow is depleted from the secondary flow and this manifests in a strong deceleration in secondary velocity, as shown in Fig. 2b. With increasing Hall parameter, the peak secondary velocity is displaced closer to the plate surface. This does not occur for the primary velocity. A weak reduction in temperatures accompanies an increase in Hall parameter (Fig. 2c), which is attributable to the inverse square effect arising in the Joule heating term in eqn. (12), viz $+\frac{2NmEc}{[\alpha_e^2+\beta_e^2]}\xi^3\left[\left(\frac{\partial F}{\partial \eta}\right)^2+G^2\right]$ – this term couples the primary and secondary velocity fields to the energy field. For non-zero Eckert number, this term has a non-trivial effect on the temperature distribution. With greater Hall parameter the thermal boundary layer is cooled and thickness is decreased.

Fig. 3a–c illustrates the effect of the ionslip parameter i.e. β_i on the primary velocity (F'), secondary velocity (G) and temperature (H) distributions through the boundary layer regime. Primary velocity is enhanced with increasing β_i (Fig. 3a). Conversely, secondary velocity and temperature are depressed with increasing values of β_i (Fig. 3b and c, respectively). Ionslip arises in the parameter, $\alpha_e = 1+\beta_i\beta e$, which causes a heating effect as the ions slip in the magnetic field [65] and a deceleration in the secondary flow. Only primary flow is positively influenced by the ionslip effect, and this characteristic is beneficial in MHD energy generator systems [66]. It is also noteworthy to mention that generally values of primary velocity are several orders of magnitude greater than secondary velocity, a familiar phenomenon in MHD flows. Similar effects have been reported by other authors, although in the absence of non-isothermal plate conditions [67,68].

Fig. 4a–c illustrates the effect of the *power law index*, *n*, on the flow characteristics. Both primary and secondary flows are decel-

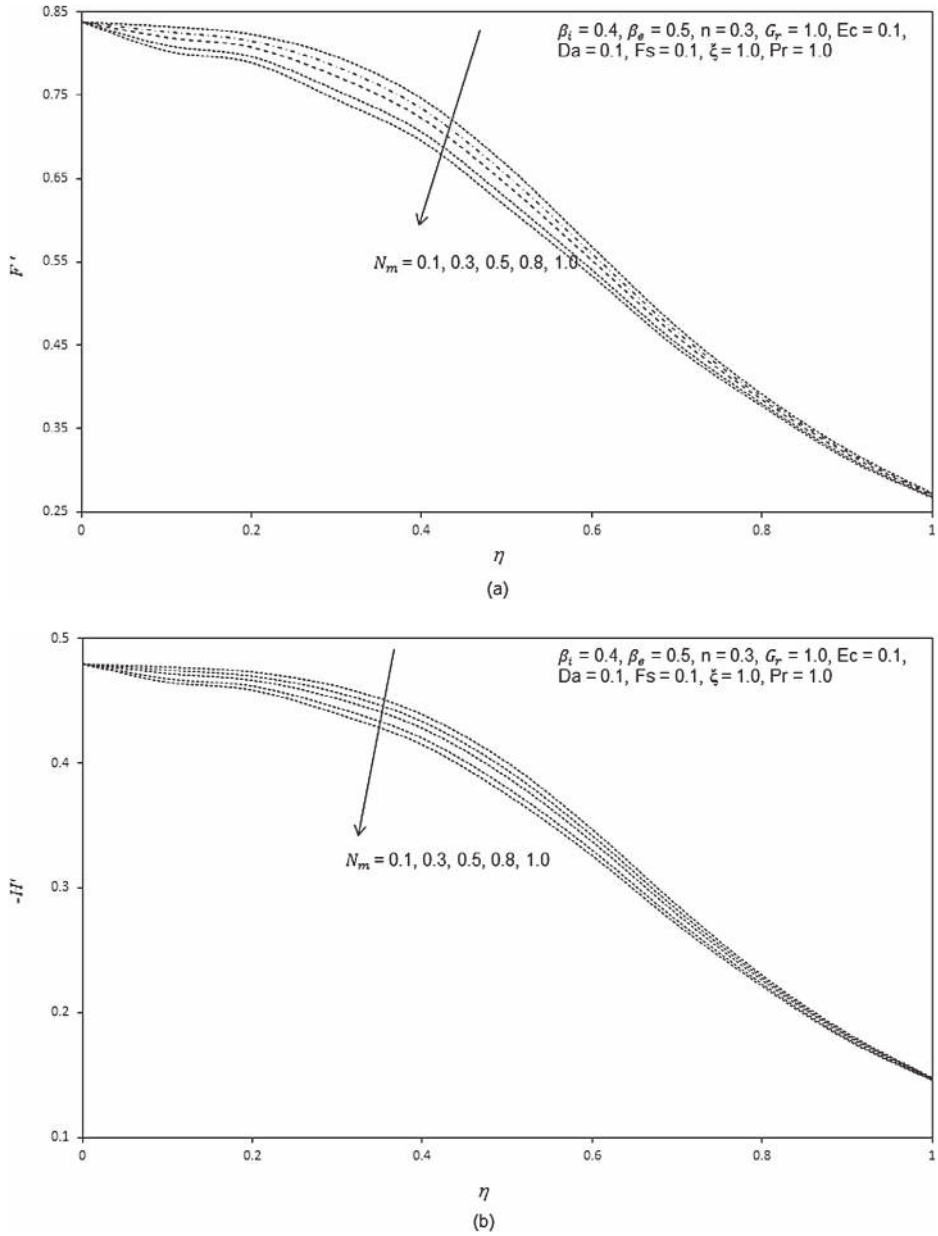

Fig. 11. (a) Influence of N_m on skin friction coefficient results. (b) Influence of N_m on Nusselt number results.

erated strongly. The parameter, n, features in many terms in all the transport equations and indeed in the wall boundary conditions. The effect is to curtail momentum development compared with the isothermal scenario. It is an important effect since non-isothermal conditions are more common in MHD generators (channel walls) than isothermal conditions. Inclusion of this effect permits engineers to avoid over-estimation of system velocities and temperatures [69]. The cooling effect of non-isothermal wall conditions is also witnessed in the significant decrease in temperatures in Fig. 4c, corresponding to a depletion in thermal boundary layer thickness. It is also pertinent to note that while the power-law index (n) does induce retardation in both primary and secondary flow fields (as do the Hall parameter and ionslip parameter on exclusively the secondary flow only), magnitudes of velocities remain positive i.e. flow reversal does not arise. The engineer must therefore select and apply transverse magnetic fields that are not excessively great (we consider nm = 0.5 in most computations reported herein), in order to mitigate possible flow reversal in MHD generator systems which can adversely influence performance efficiencies. A deeper understanding of the multiple structures in magnetohydrodynamic boundary layers can be attained with asymptotic methods and this has been reported elsewhere [70].

Fig. 5a–c presents the distribution of velocity and temperature functions for various values of the magnetic body force parameter i.e. Hartmann number, $Nm = \dfrac{\sigma B_o^2 L^{1/2}}{2\rho\nu C^2}$. An increase in Nm strongly decelerates the flow i.e., reduces primary velocity values. In all profiles a peak arises near the surface of the plate and this peak is displaced progressively closer to the wall with an elevation in Nm values. This migration phenomenon has been reported by many other researchers – see e.g. Rao and Mittal [6] and Hossain [7]. Essentially a greater retarding effect is generated in the flow with greater Nm values (i.e., stronger magnetic field strengths), which causes the prominent depression in velocities. For $Nm = 1$ the magnetic Lorentzian drag force will be of the same order of magnitude as the viscous hydrodynamic force. For $Nm > 1$, hydromagnetic drag will dominate and vice versa for $Nm < 1$. Therefore, in near-wall flows of magnetohydrodynamic generators or indeed materials processing, the flow can be very effectively controlled with a magnetic field. However, increasing *Nm* is found to accelerate the secondary velocity and the temperature. The secondary flow acceleration is beneficial in certain manipulation processes in MHD materials technology as it encourages a more homogenous constitution in materials. The increase in temperature is generated by the dissipation in supplementary work expended in dragging the fluid against the action of the magnetic field. This work is converted to thermal energy which heats the fluid and enhances thermal boundary layer thickness.

Fig. 6a–c depicts the response of primary velocity, secondary velocity and temperature to a variation in the Darcy parameter, *Da*. Primary and secondary velocities are clearly enhanced considerably with increasing *Da* as shown in Fig. 6a and b, since greater permeability of the regime corresponds to a decrease in Darcian drag force. The velocity peaks close to the plate surface are also found to be displaced further from the wall with increasing Darcy number. Porous media with greater permeability therefore assist both primary and secondary flow development whereas smaller permeability manifests in greater solid matrix impedance and decelerates both flow fields. A very strong decrease in temperature, as shown in Fig. 6c, occurs with increasing *Da* values. The progressive reduction in solid fibers in the porous medium with large *Da* values serves to decrease thermal conduction heat transfer in the regime. This inhibits the diffusion of thermal energy from the plate surface to the regime and cools the boundary layer also decreasing thermal boundary layer thickness. The presence of a porous medium therefore induces a significant effect on momentum and thermal diffusion in the system, provides a good mechanism for thermal regulation and flow control.

Fig. 7a–c presents typical profiles for velocity functions and temperature distribution for various values of Forchheimer parameter, *Fs*. An increase in *Fs* markedly *decelerates* the flow as illustrated in Fig. 7a and b, for some considerable distance into the boundary layer, transverse to the plate surface. Inertial quadratic drag has a stronger effect closer to the wall. Zueco et al. [71] have indicated that Forchheimer effects are associated with higher velocities in porous media transport. Forchheimer drag however is second order and the increase in this "form" drag effectively swamps the momentum development, thereby decelerating the flow, in particular near the plate surface. The term "non-Darcian" does not allude to a different regime of flow, but to the *amplified* effects of Forchheimer drag at higher velocities, as elaborated also in Prasad et al. [72] and Norouzi et al. [73]. With a significant increase in *Fs* there is also a slight elevation in temperatures (Fig. 7c) in the regime. Thermal boundary layer thickness is therefore weakly enhanced with greater Forchheimer effect.

Fig. 8a and b presents the influence of increasing Hall current parameter (β_e) on primary shear stress function and heat transfer rate, along with a variation in transverse coordinate (ξ). With an increase in β_e, the primary shear stress function and heat transfer rate are found to increase.

Fig. 9a and b shows the influence of increasing ionslip parameter (β_i) on primary shear stress function and heat transfer rate, along with a variation in transverse coordinate (ξ). Increasing β_i is observed to increase the primary shear stress function and heat transfer rate.

Fig. 10a and b documents the effect of increasing power law index (n) on primary shear stress function and heat transfer rate, along with a variation in transverse coordinate (ξ). It is observed that increasing n decreases the primary whereas it increases the heat transfer rate.

Fig. 11a and b presents the influence of increasing Hartmann (magnetic body force) number (N_m) on primary shear stress function and heat transfer rate, along with a variation in transverse coordinate (ξ). It is observed that increasing N_m decreases primary and heat transfer rate. This verifies earlier computations showing that the flow is retarded with magnetic field but the fluid is heated. The transport of heat from the fluid to the plate corresponds to greater heat transfer rates and a drop in fluid temperature.

The influence of selected parameters on the wall shear stress functions and Nusselt number (heat transfer rate) are documented in Tables 1 and 2.

Table 1 presents the influence of increasing Darcy number (*Da*) on primary shear stress function, secondary shear stress function and heat transfer rate, along with a variation in transverse coordinate (ξ). Increasing *Da* is observed to increase all the parameters i.e., the primary and secondary shear stress functions are elevated since both primary and secondary flow is accelerated whereas the heat transfer rate is enhanced due to the decrease in temperature in the fluid leading to greater thermal energy transport to the plate.

Table 2 presents the influence of increasing Forchheimer quadratic drag number (*Fs*) on primary shear stress function, secondary shear stress function and heat transfer rate, along with a variation in transverse coordinate (ξ). Increasing *Fs* is observed to depress primary shear stress function and secondary shear stress function (due to flow acceleration) but enhances Nusselt number (heat transfer rate).

10. Conclusions

A mathematical model has been developed for the steady hydromagnetic free convection heat transfer of an electrically-conducting fluid from a non-isothermal vertical sheet adjacent to a non-Darcian porous medium in the presence of Hall currents, ionslip currents and viscous and Joule heating effects. The boundary value problem (BVP) has been transformed from an (x, y, z) coordinate system to a (ξ,η) coordinate system. A number of important special cases have been described in addition to key engineering parameters being derived. The Keller box method (KBM) has been employed to obtain implicit finite difference numerical solutions for the solution of the strongly coupled, nonlinear two-point boundary value problem. Extensive computations have been presented for the effects of *power-law thermal index (n), Darcy number (Da), Forchheimer number (Fs), hydromagnetic parameter (Nm), Hall current parameter (β_e), ionslip parameter (β_i),* on the velocity fields and temperature distribution in the regime, with prescribed *Eckert number (Ec)* and *Prandtl number (Pr)*. Computations have been validated with Nakamura's tridiagonal difference method (NTM). A strong deceleration in primary and secondary flow has been shown to arise with greater non-isothermal effect at the wall, also leading to a decrease in temperatures. Increasing Hall parameter and ionslip are observed to accelerate weakly the primary flow but to strongly retard the secondary flow. Increasing Darcy number accelerates both primary and secondary flow but cools the fluid, as does an increase in Forchheimer number. The current study finds applications in both magnetic materials fabrication (e.g. liquid metal flows) and MHD energy generator near-wall flows. It also renders some useful benchmarks for more generalized commercial CFD simulations. The study has considered Newtonian fluids. Future investigations will address non-Newtonian working fluids e.g. Maxwell viscoelastic fluids and will be reported imminently.

Nomenclature

b	Forchheimer form-drag parameter
$\mathbf{B_0}$	Magnetic field
C_f	Skin friction coefficient
c_p	Specific heat parameter
Da	Darcy parameter

De	Deborah number
D_m	Mass (species) diffusivity
Ec	Eckert number
F	Non-dimensional steam function
Fs	Forchheimer parameter
G	Dimensionless lateral velocity
Gr_x	Grashof number
g	Acceleration due to gravity
H	Dimensionless temperature function
J	Electric current density
K	Permeability of the porous medium
k	Thermal conductivity of fluid
L	Characteristic length
m_e	Electron mass
n_e	Electron number density
n	Power-law exponent
Nm	Magnetic body force parameter
Nu_x	Local Nusselt number
Pr	Prandtl number
$q_w(x)$	Local heat transfer coefficient
t_e	Electron collision time
T	Temperature of the fluid
$T_w(x)$	Variable wall temperature
T	Cauchy stress tensor
u, v, w	Non-dimensional velocity components along the x, y and z directions, respectively
U	velocity
V	Velocity vector
x	Stream wise coordinate
y	Transverse coordinate

Greek symbols

α	Thermal diffusivity
β_i	Ion-slip parameter
β	The coefficient of volume expansion
β_e	Hall current parameter
ω_e	Electron frequency
η	The dimensionless radial coordinate
μ	Dynamic viscosity of the partially-ionized fluid
ν	Kinematic viscosity
ρ	Density of the fluid
σ^*	The Stefan–Boltzmann constant
ξ	The dimensionless tangential coordinate
ψ	Dimensionless stream function

Subscripts

w	Conditions on the wall (sphere surface)
∞	Free stream conditions

References

[1] W.C. Kennedy, W.F. Hughes, The steady state performance, magneto-acoustical response and stability of flow in a Hall MHD generator, Int. J. Eng. Sci. 11 (11) (1973) 1143–1160.
[2] M.J. Uddin, O.A. Bég, N.S. Amin, Hydromagnetic transport phenomena from a stretching or shrinking nonlinear nanomaterial sheet with Navier slip and convective heating: a model for bio-nano-materials processing, J. Magn. Magn. Mater. 368 (2014) 252–261.
[3] F.-C. Li, T. Kunugi, A. Serizawa, MHD effect on flow structures and heat transfer characteristics of liquid metal–gas annular flow in a vertical pipe, Int. J. Heat Mass Transfer 48 (12) (2005) 2571–2581.
[4] O.A. Bég, M.M. Hoque, M. Wahiuzzaman, M. Mahmud, M. Ferdows, Spectral numerical simulation of laminar magneto-physiological Dean flow, J. Mech. Med. Biol. 14 (3) (2014) 18.
[5] B.S. Mazumder, Combined effects of Hall currents and rotation on hydromagnetic flow over an oscillating porous plate, Int. J. Eng. Sci. 15 (1977) 601–606.
[6] B.N. Rao, M.L. Mittal, Magnetohydrodynamic boundary layer on a wedge, ASME J. Appl. Mech. 48 (1981) 656–659.
[7] M.A. Hossain, Effect of Hall current on unsteady hydromagnetic free convection flow near an infinite vertical porous plate, J. Phys. Soc. (Japan) 55 (7) (1986) 2183–2190.
[8] T.L. Raju, V.V.R. Rao, Hall effects on temperature distribution in a rotating ionized hydromagnetic flow between parallel walls, Int. J. Eng. Sci. 31 (7) (1993) 1073–1091.
[9] E. Sawaya, N. Ghaddar, F. Chaaban, Evaluation of the Hall parameter of electrolyte solutions in thermosyphonic MHD flow, Int. J. Eng. Sci. 31 (7) (1993) 1073–1091.
[10] R. Bhargava, H.S. Takhar, Effect of Hall currents on the MHD flow and heat transfer of a second order fluid between two parallel porous plates, J. MHD Plasma Space Res. 10 (2001) 73–87.
[11] K.R. Cramer, S.-I. Pai, Magnetofluid Dynamics for Engineers and Applied Physicists, McGraw-Hill, New York, 1973.
[12] V.M. Soundalgekar, N.V. Vighnesam, H.S. Takhar, Hall and ion-slip effects in the MHD Couette flow with heat transfer, IEEE Trans. Plasma Sci. 7 (1979) 178–182.
[13] P.C. Ram, H.S. Takhar, MHD free convection from an infinite vertical plate in a rotating fluid with Hall and ionslip currents, Fluid Dyn. Res. 11 (1993) 99–105.
[14] P.C. Ram, A. Singh, H.S. Takhar, Effects of Hall and ionslip currents on convective flow in a rotating fluid with a wall temperature oscillation, J. Magnetohydrodyn. Plasma Res. 5 (1995) 1–16.
[15] H.S. Takhar, B.K. Jha, Effects of Hall and ion-slip currents on MHD flow past an impulsively started plate in a rotating system, J. Magnetohydrodyn. Plasma Res. 8 (1998) 61–72.
[16] E.F. Elshehawey, N.T. Eldabe, E.M. Elbarbary, N.S. Elgazery, Chebyshev finite-difference method for the effects of Hall and ion-slip currents on magneto-hydrodynamic flow with variable thermal conductivity, Can. J. Phys. 82 (9) (2004) 701–715.
[17] M. Turkyilmazoglu, Exact solutions for the incompressible viscous magnetohydrodynamic fluid of a porous rotating disk flow with Hall current, Int. J. Mech. Sci. 56 (1) (2012) 86–95.
[18] M. Turkyilmazoglu, Exact solutions for the incompressible viscous magnetohydrodynamic fluid of a rotating disk flow with Hall current, Int. J. Non Linear Mech. 46 (8) (2011) 1042–1048.
[19] I. Michiyoshi, R. Matsumoto, Heat transfer by Hartmann's flow in thermal entrance region, Int. J. Heat Mass Transfer 7 (1964) 1.
[20] R.-S. Wu, K.C. Cheng, Thermal entrance region heat transfer for MHD laminar flow in parallel plate channels with unequal wall temperatures, Heat Mass Transfer J. 9 (4) (1976) 273–280.
[21] M.A. Mansour, R.S.R. Gorla, Joule heating effects on unsteady natural convection from a heated vertical plate in a micropolar fluid, Can. J. Phys. 76 (12) (1998) 977–984.
[22] O.A. Bég, Computational fluid dynamic (Spectral DTM) simulation of Hartmann flow with Joule heating: applications in liquid metal processing, Technical Report, GORT Engovation Aerospace Research, Bradford, November, UK, 2012.
[23] W.A. Aissa, A.A. Mohammadein, Joule heating effects on a micropolar fluid pasta stretching sheet with variable electric conductivity, J. Comput. Appl. Mech. 6 (1) (2005) 3–13.
[24] S.K. Ghosh, O.A. Bég, A. Aziz, A mathematical model for magnetohydrodynamic convection flow in a rotating horizontal channel with inclined magnetic field, magnetic induction and Hall current effects, World J. Mech. 1 (3) (2011) 137–154.
[25] H.M. Duwairi, Viscous and Joule heating effects on forced convection flow from radiate isothermal porous surfaces, Int. J. Num. Meth. Heat Fluid Flow 15 (5) (2005) 429–440.
[26] J. Zueco, O.A. Bég, L.M. Lopez-Ochoa, Non-linear transient hydromagnetic partially ionised dissipative Couette flow in a non-Darcian porous medium channel with Hall, ionslip and Joule heating effects, Prog. Comput. Fluid Dyn. 11 (2) (2011) 116–129.
[27] M. Rahimi-Gorji, O. Pourmehran, M. Gorji-Bandpy, D.D. Ganji, An analytical investigation on unsteady motion of vertically falling spherical particles in non-Newtonian fluid by Collocation Method, Ain. Shams. Eng. J. 6 (2) (2014) 531–540 http://dx.doi.org/10.1016/j.asej.2014.10.016.
[28] O. Pourmehran, M. Rahimi-Gorji, M. Gorji-Bandpy, T.B. Gorji, Simulation of magnetic drug targeting through tracheobronchial airway in presence of an external nonuniform magnetic field using Lagrangian magnetic particle tracking, J. Magn. Magn. Mater. (1) (2015) 380–393.
[29] O. Pourmehran, M. Rahimi-Gorji, M. Gorji-Bandpy, D.D. Ganji, Analytical investigation of squeezing unsteady nanofluid flow between parallel plates by LSM and CM, Alexandria Eng. J. 54 (1) (2015) 17–26.
[30] M. Rahimi-Gorji, O. Pourmehran, M. Hatami, D.D. Ganji, Statistical optimization of microchannel heat sink (MCHS) geometry cooled by different nanofluids using RSM analysis, Eur. Phys. J. Plus 130 (22) (2015) 121.
[31] B. Gebhart, J. Mollendorf, Viscous dissipation in external natural convection flows, J. Fluid Mech. 38 (1969) 97.
[32] V.M. Soundalgekar, I. Pop, Viscous dissipation effects on unsteady free convective flow past an infinite vertical porous plate with variable suction, Int. J. Heat Mass Transfer 17 (1) (1974) 85–92.
[33] V. Javeri, Combined influence of Hall effect, ion slip, viscous dissipation and Joule heating on MHD heat transfer in a channel, Heat Mass Transfer 8 (3) (1975) 193–303.
[34] H.S. Takhar, V.M. Soundalgekar, Dissipation effects on MHD free convection flow past a semi-infinite vertical plate, Appl. Sci. Res. 36 (1980) 163–171.
[35] D.L. Turcotte, D.A. Spence, H.H. Bau, Multiple solutions for natural convective flows in an internally heated, vertical channel with viscous dissipation and pressure work, Int. J. Heat Mass Transfer 25 (5) (1982) 699–706.

[36] T. Basu, D.N. Roy, Laminar heat transfer in a tube with viscous dissipation, Int. J. Heat Mass Transfer 28 (3) (1985) 699–701.
[37] A. Barletta, Laminar mixed convection with viscous dissipation in a vertical channel, Int. J. Heat Mass Transfer 41 (22) (1998) 3501–3513.
[38] A. Barletta, E. Rossi di Schio, Effect of viscous dissipation on mixed convection heat transfer in a vertical tube with uniform wall heat flux, Heat Mass Transfer J. 38 (1) (2001) 129–140.
[39] K.S. Chen, J.R. Ho, Effects of flow inertia on vertical, natural convection in saturated porous media, Int. J. Heat Mass Transfer 29 (5) (1986) 753–759.
[40] D.M. Manole, J.L. Lage, The inertia effect on natural convection within a fluid saturated porous medium, Int. J. Heat Fluid Flow 14 (1993) 376–384.
[41] O. Pourmehran, M. Rahimi-Gorji, M. Hatami, S.A.R. Sahebi, G. Domairry, Numerical optimization of microchannel heat sink (MCHS) performance cooled by KKL based nanofluids in saturated porous medium, J. Taiwan Inst. Chem. Eng. (2015) http://dx.doi.org/10.1016/j.jtice.2015.04.016.
[42] O.A. Bég, O.D. Makinde, Viscoelastic flow and species transfer in a Darcian high-permeability channel, J. Petrol. Sci. Eng. 76 (2011) 93–99.
[43] H.B. Keller, Numerical methods in boundary-layer theory, Ann. Rev. Fluid Mech. 10 (1978) 417–433.
[44] C. Rossi, M.D. Rouhani, D. Esteve, Prediction of the performance of a Si-micromachined microthruster by computing the subsonic gas flow inside the thrusters, Sens. Actuators 87 (2000) 96–104.
[45] P. Sturdza, An aerodynamic design method for supersonic natural laminar flow aircraft. PhD Thesis, Dept. Aeronautics and Astronautics, Stanford University, California, USA, December (2003).
[46] J.-P. Croisille, Keller's box-scheme for the one-dimensional stationary convection-diffusion equation, Computing 68 (1) (2002) 37–63.
[47] V.R. Prasad, B. Vasu, O.A. Bég, Thermo-diffusion and diffusion-thermo effects on MHD free convection flow past a vertical porous plate embedded in a non-Darcian porous medium, Chem. Eng. J. 173 (2011) 598–606.
[48] M. Narayana, P. Sibanda, S.S. Motsa, P.G. Siddheshwar, On double-diffusive convection and cross diffusion effects on a horizontal wavy surface in a porous medium, Boundary Value Probl. 88 (2012) 1–22.
[49] M.I. Anwar, I. Khan, S. Sharidan, M.Z. Salleh, Conjugate effects of heat and mass transfer of nanofluids over a nonlinear stretching sheet, Int. J. Phys. Sci. 7 (2012) 4081–4092.
[50] J.-J. Shu, G. Wilks, Heat transfer in the flow of a cold, two-dimensional draining sheet over a hot, horizontal cylinder, Eur. J. Mech. B/Fluids 26 (2007) 1–5.
[51] F.M. Ali, R. Nazar, N.M. Arifin, I. Pop, Unsteady shrinking sheet with mass transfer in a rotating fluid, Int. J. Num. Meth. Fluids 66 (2011) 1465–1474.
[52] A. Kaya, Heat and mass transfer from a horizontal slender cylinder with a magnetic field effect, Therm. Sci. Technol. 31 (2) (2011) 73–78.
[53] B.V.R. Kumar, S.V.K. Murthy, Soret and Dufour effects on double-diffusive free convection from a corrugated vertical surface in a non-Darcy porous medium, Transp. Porous Media 85 (2010) 117–130.
[54] V. Esfahanian, F. Torabi Numerical simulation of lead–acid batteries using Keller–box method, Lead-Acid Batteries (LABAT) Conference, Sofia, Bulgaria, June (2005).
[55] S. Abdul Gaffar, V.R. Prasad, O.A. Bég, Computational analysis of magnetohydrodynamic free convection flow and heat transfer of non-Newtonian tangent hyperbolic fluid from a horizontal circular cylinder with partial slip, Int. J. Appl. Comput. Math. (2015) doi:10.1007/s40819-015-0042-x.
[56] T. Cebeci, P. Bradshaw, Momentum Transfer in Boundary Layers, Hemisphere, Washington, 1977.
[57] S. Nakamura, Applied Numerical Methods and Software, Prentice-Hall, NJ, USA, 1995.
[58] R.S.R. Gorla, A. Slaouti, H.S. Takhar, Free convection in micropolar fluids over a uniformly heated vertical plate, Int. J. Num. Meth. Heat Fluid Flow 8 (1998) 504–518.
[59] I. Pop, S. Nakamura, Laminar boundary layer flow of power-law fluids over wavy surfaces, Acta Mech. 115 (1996) 55–65.
[60] O.A. Bég, Computational hemodynamics for hybrid heart pump devices- finite element and Nakamura difference simulations, Technical Report, Gort Engovation, HEMO-1-4-13, 128 pages, March (2013).
[61] O.A. Bég, T.A. Bég, H.S. Takhar, A. Raptis, Mathematical and numerical modeling of non-Newtonian thermo-hydrodynamic flow in non-Darcy porous media, Int. J. Fluid Mech. Res. 31 (2004) 1–12.
[62] O.A. Bég, V.R. Prasad, B. Vasu, Numerical study of mixed bioconvection in porous media saturated with nanofluid containing oxytactic micro-organisms, J. Mech. Med. Biol. (2014) doi:10.1142/S021951941350067X.
[63] O.A. Bég, J. Zueco, M. Norouzi, M. Davoodi, A.A. Joneidi, A.F. Elsayed, Network and Nakamura tridiagonal computational simulation of electrically-conducting biopolymer micro-morphic transport phenomena, Comput. Biol. Med. 44 (2014) 44–56.
[64] G.W. Sutton, A. Sherman, Engineering Magneto-Hydrodynamics, McGraw-Hill, New York, 1965.
[65] L.S. Dzung, MHD generators with ion slip and finite electrode segments, Symposium on Magnetohydrodynamic Electrical Power Generation; Salzburg (Austria); 4–8 Jul, (1966) 177–184.
[66] T. Hardianto, N. Harada, Three-dimensional flow analysis in a Faraday-type MHD generator, IEEE Trans. Ind. Appl. 44 (2008) 90–100.
[67] G.W. Sutton, R. Robben, Preliminary experiments on MHD channel flow in ionized gas, Proc. Eleventh Int. Symposium, Polytechnic Institute of Brooklyn, Brooklyn, New York, vol. XI (1961) 307–321.
[68] N.S. Elgazery, The effects of chemical reaction, Hall and ion slip currents on MHD flow with temperature dependent viscosity and thermal diffusivity, Commun. Nonlin. Sci. Numer. Simul. 14 (2009) 1267–1283.
[69] F.A. Lyman, A.W. Goldstein, J.E. Heighway, Effect of Seeding and Ion Slip on Electron Heating in a Magnetohydrodynamic Generator, NASA TN D-2118, NASA Glenn Research Centre, California, 1964.
[70] W.R. Sears, The boundary layer in a crossed-field MHD, J. Fluid Mech. 25 (1966) 229–240.
[71] O.A. Bég, J. Zueco, S.K. Ghosh, Unsteady hydromagnetic natural convection of a short-memory viscoelastic fluid in a non-Darcian regime: network simulation, Chem. Eng. Commun. 198 (2010) 172–190.
[72] V.R. Prasad, S.A. Gaffar, O.A. Bég, Non-similar computational solutions for free convection boundary-layer flow of a nanofluid from an isothermal sphere in a non-Darcy porous medium, J. Nanofluids 4 (2015) 1–11.
[73] M. Norouzi, M. Davoodi, O.A. Bég, An analytical solution for convective heat transfer of viscoelastic flows in rotating curved pipes, Int. J. Therm. Sci. 90 (2015) 90–111.